Estimation of Compressibility Factor of Saturated Liquid and Vapor of Bulk and Nanoconfined Methane

A Dissertation

Submitted in the partial fulfillment of the requirements for the award of degree of

Masters of Sciences

In

Chemistry

Submitted By

Simran

(Roll No.301702034)

Under the Supervision of

Dr. Sudhir K Singh

(Associate Professor)

Department of Chemical Engineering

School of Chemistry and Biochemistry

Thapar Institute of Engineering and Technology

Patiala, 147004

June 2019

CANDIDATE' s DECLARATION

I hereby declare that the work being presented in the dissertation entitled "Estimation of compressibility factor of saturated liquid and vapor of bulk and nanoconfined methane" in partial fulfillment of the requirements for the award of degree of Masters of Science in Chemistry and being submitted to School of Chemistry and Biochemistry, Thapar institute of engineering and technology, Patiala, is my own work during the period of January to June 2019, under the supervision of **Dr. Sudhir K Singh**. I have not submitted embodied in this dissertation for the award of any other degree.

Simran.

Patiala **Simran**

Date: 9/8/2019

This is certify that the above statement made by the candidate is correct and true to the best of our knowledge.

Sudhir Kr. Singh.

Dr Sudhir K Singh

Associate Professor,
Department of Chemical Engineering,
TIET, Patiala-147004

ACKNOWLEDGEMENT

First of all, I owe my gratitude to the Head of the Department, **Dr. Amjad Ali** for providing me the opportunity in the form of this dissertation to develop my interest in research.

In the same spirit, I would like to thank my Supervisor, **Dr. Sudhir K Singh** for his constructive guidance and constant support during the project. The work presented here could not have been accomplished without their patience and ever willingness to teach. They have taught me to concise and correct in my approach from the formulation of ideas to the presentation of the results.

Special thanks to all the **Teaching Faculty** of the department for their cooperation and guidance.

I am grateful to **TIET & School of chemistry and biochemistry** for providing financial support and all necessary infrastructure and laboratory facilities to carry out the experimental work.Words fail me to express my thanks to my family and friends who have always supported me and have been a source of strength and inspiration to me during the entire period of the work. All the thanks are, however, only fraction of what is due to almighty for granting me.

ABSTRACT

In this work, compressibility factor of saturated liquid, saturated vapor and critical compressibility factor of bulk and confined methane are investigated. We have first comparedthe experimental data of compressibility factor of saturated liquid, saturated vapor and critical compressibility factor with the corresponding simulation data of current work.The experimental compressibility factor of saturated liquid and vapor and critical compressibility factor are in good agreement with the data obtained using molecular simulation approach of current work. Further, we have estimated the compressibility factor of saturated liquid and saturated vapor of nanoconfined methane at various reduced temperatures in a given pore width. Estimated compressibility factor of saturated liquid increases with increase in temperature and the compressibility factor of saturated vapor decreases with increases in temperature for all studied nanopore width, H = 40Å to 5.4Å. It has been observed that with increase in reduced temperature, change in compressibility factor of saturated liquid is comparatively less than the change in compressibility factor of saturated vapor. Critical compressibility factor is estimated for all studied nanopore width using critical point data obtained from the simulation.Critical compressibility factor of bulk methane and methane confined in 40Ånanopore width are approximately same. Further from 30Åto 8Ånanopore width critical compressibility factor is monotonically decreasing and then from 8Å to 5.4Ånanopore width it remains indifferent reflecting quasi-2D behaviour of nanoconfined methane.

Key words: Compressibility factor, Monte Carlo simulation, Methane, Nanoconfinement, Pore width.

LIST OF CONTENTS

CHAPTER-1

INTRODUCTION

1.1 Compressibility Factor

The deviation from ideal-gas behaviour at a given temperature and pressure can accurately be accounted for by the introduction of a correction factor called the compressibility factor. Compressibility factor is generally explained by the three factors pressure, volume and temperature. The equation of state for the gaseous phase is ordinarily written as, PV = ZRT where Z denotes the compressibility factor and R is universal gas constant. The Z factor for all gases is approximately same at the same reduced pressure and temperature. For vapor-liquid phase equilibria of single component, the compressibility factor of saturated liquid (Z_l) and saturated vapor (Z_g) is defined as

$$\boldsymbol{Z_l = \frac{Pv_l}{RT} = \frac{P}{\rho_l RT}} \quad (1)$$

$$\boldsymbol{Z_g = \frac{Pv_g}{RT} = \frac{P}{\rho_g RT}} \quad (2)$$

In thermodynamics, cubic equation of states are extensively used to predict the thermodynamic properties of fluids. The compressibility factor (Z) for such cubic equations of states can be written as [1]

$$Z^3 + \alpha Z^2 + \beta Z + \gamma = 0 \quad (3)$$

Where $Z = \frac{Pv}{RT}$

Cardan's method, which is explained below can be used to estimate the roots of equation 3 as follows,

$$\alpha = -1 - B + uB \quad (4)$$

$$\beta = A + wB^2 - uB - uB^2 \quad (5)$$

$$\gamma = -AB - wB^2 - wB^3 \quad (6)$$

$$A = \frac{\alpha P}{RT^2} \quad (7)$$

$$B = \frac{bP}{RT} \quad (8)$$

Substitute

$$Z = X - (\frac{\alpha}{3}) \quad (9)$$

In equation 3 to get

$$X^3 + pX + q = 0 \quad (10)$$

Where $p = \beta - (\frac{\alpha^2}{3})$

$$q = \left(\frac{2\alpha^3}{27}\right) - \left(\frac{\alpha\beta}{3}\right) + \gamma \quad (11)$$

Let $D = \left(\frac{q^2}{4}\right) + (\frac{p^3}{27})$ (12)

If D > 0 there is only one real root and it is given by

$$Z = \{-\frac{q}{2} + \sqrt{D}\}^{\frac{1}{3}} + \left\{-\frac{q}{2} - \sqrt{D}\right\}^{\frac{1}{3}} - \frac{\alpha}{3} \quad (13)$$

If D = 0, there are three real roots and two of them are equal. They are given by

$$Z_1 = -2(\frac{q}{2})^{\frac{1}{3}} - \frac{\alpha}{3} \quad (14)$$

$$Z_2 = Z_3 = (\frac{q}{2})^{\frac{1}{3}} - \frac{\alpha}{3} \quad (15)$$

If D < 0, there are unequal three roots. They are given by

$$Z_1 = 2r^{\frac{1}{3}} \cos(\frac{\theta}{3}) - \frac{\alpha}{3} \quad (16)$$

$$Z_2 = 2r^{\frac{1}{3}} \cos(\frac{2\pi+\theta}{3}) - \frac{\alpha}{3} \quad (17)$$

$$Z_3 = 2r^{\frac{1}{3}} \cos\left(\frac{4\pi+\theta}{3}\right) - \frac{\alpha}{3} \quad (18)$$

Where $\cos\theta = -\frac{q}{2}\left(\frac{27}{p^3}\right)^{\frac{1}{2}}$ (19)

$$r = \left(\frac{-p^3}{27}\right)^{\frac{1}{2}} \quad (20)$$

The value of u, w, α,β,γ for the different cubic equation of states(EOS) are different. Following table shows the value of u, w, α, β, γ for the different cubic EOS.

Table1: Value of u, w, α, β, γ for the cubic equation of state (EOS)

Equation of state	**u**	**w**	**α**	**β**	**γ**
Vander Walls	0	0	-1-B	A	-AB
Redich-Kwong (RK)	1	0	-1	$A-B-B^2$	-AB
Soave-Redich-Kwong (SRK)	1	0	-1	$A-B-B^2$	-AB
Peng-Robinson (PR)	2	-1	-1+B	$A-2B-3B^2$	$-AB+B^2+B^3$

From above equations it is evident that if D = 0, there are three real roots of Z, out of which two are equal and they denote the critical compressibility factor, Z_c. However, If D < 0, there are unequal three roots. Out of these three roots the least value denotes the compressibility factor of saturated liquid (Z_l) and highest value denotes the compressibility factor of saturated vapor (Z_g). The other value of Z, which is in between Z_l and Z_g, does not exist practically.

In the current work, compressibility factor of saturated liquid (Z_l) and saturated vapor (Z_g) of bulk methane and nanoconfined methane are estimated using the simulation data (saturation temperature T, saturation pressure P, saturated liquid density ρ_l, and saturated vapor density ρ_g) obtained from grand canonical transition-matrix Monte Carlo (GC-TMMC) simulations. Critical compressibility factors of bulk methane and nanoconfined methane are estimated using the critical point data obtained from simulations.

1.2 Nanoconfined fluid

Fluids confined by solid surfaces with separation distances of the order of few molecular diameters are known as nanoconfined fluid. Nanoconfined fluids are of great importance in industrial applications. This includes emerging areas[2-5] such as ionic liquid-based supercapacitors. When molecules are confined in such small pores, their thermodynamic behavior can be reasonably different from that of the corresponding bulk fluid.[2,6] In some earlier work, Gubbins and coworkers[7] performed grand-canonical Monte Carlo (GCMC) simulations with umbrella sampling on the Lennard-Jones fluid confined between smooth walls. The fluids are replicate between parallel solid surfaces with varying pore sizes and wall-fluid interaction potential. The fluid-solid phase transition mode has been characterized through determination of the heat capacity. The results indicate that for pores of ideal-spacing, the order-disorder transition temperature is reduced as the pore size increases until values consistent with that seen in a bulk system.

The structure and properties of fluids confined in pores may show an affecting separation from macroscopic bulk fluids. The main reason for this change lies in the presence of system walls. In addition to the entropic wall effect, system walls can naturally change the energy of the confined fluid compared to bulk fluids. The efficiency effect of the walls on a confined fluid appears in two forms. The first effect is the isolate of the intermolecular interactions by the walls, which appears for example in the integrals for calculation of the thermodynamic properties. The second wall effect concern the surface-molecule interactions. In such nanoconfined fluids, the presence of wall forces and the competition between fluid-wall and fluid-fluid forces could lead to important thermodynamic properties, including new kinds of phase transitions not observed in the macroscopic fluid systems. In this work investigators have used the perturbative fundamental measure density functional theory to study energy effects on the structure and properties of a hard core Yukawa fluid confined in a slit pore. These results show the changes undergone by the structure and phase transition of the nanoconfined fluids as a result of energy effects.

1.3 Objective

Objective of current work is as follows:

- Estimation of compressibility factor of saturated liquid and saturated vapor of bulk methane using the data obtained from Grand Canonical Transition Matrix Simulations.
- Estimation of critical compressibility factor of Bulk methane.
- Comparison of above compressibility factor of saturated liquid & saturated vapor and critical compressibility factor of bulk methane from experimental data.
- Estimation of compressibility factor of saturated vapor and liquid of methane confined in different nanopore width of graphite slit pore.
- Estimation of critical compressibility factor of methane in different nanopore width of graphite slit pore.

CHAPTER-2

Review of Literature

Largo J*et al.*[8] has worked on the first-order perturbative contribution to the compressibility factor of square-well (SW) fluids from Monte Carlo simulation and integral equation theory. In this work they studied canonical ensemble Monte Carlo simulations. The zero- and first-order terms in the expansion of the compressibility factor of SW fluids in the power series of the inverse of the reduced temperature for different densities and well widths. In addition, the values of the compressibility factor obtained from the perturbative expansion, truncated beyond the first-order term, are compared with those obtained directly by Monte Carlo simulations performed on the SW system, which were reported previously. The aim of their work is to establish the limits of validity of this truncated expansion in terms of densities, temperatures, and potential widths. In this work they have found that this approximation is very accurate for any value of the potential width, density, and temperature, except perhaps for small potential widths at very low temperatures. Moreover, the values of the first-order contribution are compared with those obtained from the Tang and Lu[9] perturbation theory based on the integral equation theory as well as with those from the Barker-Henderson perturbation theory. The aim is two-fold: on one hand, to establish whether the pressure route used in the Tang-Lu theory provides better accuracy than the energy route used in the Barker-Henderson theory and on the other hand to determine whether the Tang-Lu theory, which is more complicated, is advantageous compared to the Barker-Henderson theory. In this work they have found that the Barker-Henderson perturbation theory is advantageous compared to the Tang-Lu theory with regard to the calculation of the thermodynamic properties, whereas the contrary is true for structural properties. In another work[10] researchers have worked using compressibility factor as a predictor of confined hard-sphere fluid dynamics. They studied the correlations between the diffusivity and the compressibility factor of bulk hard sphere fluid as predicted by the ultra-local limit of the barrier hopping theory. Their specific aim is to determine if these correlations observed in the bulk equilibrium hard-sphere fluid can be used to predict the self-diffusivity of fluid confined between a slit-pore or a rectangular channel. In this work, they consider a single-component and a binary mixture of hard spheres. To represent confining walls, they use purely reflecting hard walls and

interacting square-well walls. Their results clearly show that the correspondence between the diffusivity and the compressibility factor can be used along with the knowledge of the confined fluid's compressibility factor to predict its diffusivity with quantitative accuracy. This work also suggests that a simple measure, the average fluid density, can be an accurate predictor of confined fluid diffusivity for very tight confinements (few particle diameters wide) at low to intermediate density conditions. Together, these results provide further support for the idea that one can use robust connections between thermodynamic and dynamic quantities to predict dynamics of confined fluids from their thermodynamics. Further in a work [11]investigators has worked on virial expansion providing of the linearity for a unit compressibility factor. They showed that the law of linearity for a unit compressibility factor testifying a lot of experimental data for many substances can be provided by appropriate procedure following from the rigorous consequences of statistical mechanics, namely, the virial expansion. An equation of state (EOS) that includes the terms up to the fourth power of density is obtained by using second and third virial coefficients. The critical point parameters, phase densities, and pressure along the liquid-gas coexistence curve for the Lennard-Jones (LJ, 6-12) and exp-6 Buckingham potentials are defined. The results corresponding to the LJ potentials are in good agreement with the solution of integral equations and simulation results. For the Buckingham potentials, their predictions agree well with the experimental data for the group of real substances, satisfying the law of corresponding states.

CHAPTER-3

METHEDOLOGY

3.1 Potential Model

In this work united atom approach[12] is used to model the methane molecule. Methane-methane interactions are described with the Buckingham exponential-6 intermolecular potential[13].The pair interaction energy, *U*, for exponential-6 intermolecular potential is represented by following equation. The interaction energy between methane-methane molecules are shown in figure 1.

$$U(r) = \left\{ \frac{\varepsilon}{1 - 6/\alpha} \left[\frac{6}{\alpha} \exp\left(\alpha \left[1 - \frac{r}{r_m} \right] \right) - \left(\frac{r_m}{r} \right)^6 \right] \right\} \quad \text{for} \quad r > r_{\max}$$
$$= \infty \quad \text{for} \quad r < r_{\max} \qquad (21)$$

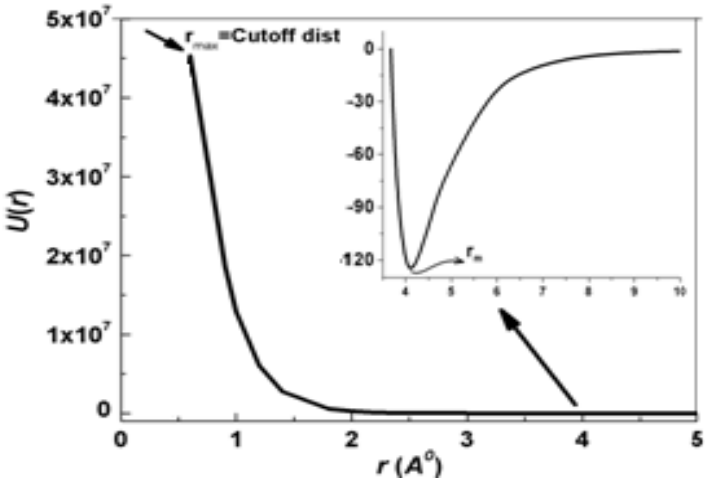

Fig.1 Interaction Potential between methane-methane molecule

where ε, r_m and α are interaction potential parameters. The variable r_m is radial distance at which U(r) reaches a minimum, and the cutoff distance r_{max} represents the smallest radial distance for which d[U(r)]/d(r)=0. The radial distance for which U(r) = 0 is denoted by σ, which is same as the diameter of the methane (CH_4) molecule. The parameters ε, σ and α for CH_4 are 160.3K, 3.73 Å, and 15 respectively.

In this work, nanopore is of slit geometry with smooth surfaces. In the current work wall-fluid interaction is described by the 9-3 Steele potential[14]

$$\varphi_{wf}(z) = 2/3\pi\rho_w\varepsilon_{wf}{\sigma_{wf}}^3\{\frac{2}{15}\left(\frac{\sigma_{wf}}{z}\right)^9 - \left(\frac{\sigma_{wf}}{z}\right)^3\} \quad (22)$$

where z is the distance of the fluid particle from the wall surface and ρ_w, ε_{wf}, and σ_{wf} are the parameters of the Steele potential. For methane, σ_{wf} for graphite surface is 3.7995 Å.[15] Following figure shows the interaction potential between graphite surface and methane molecule.

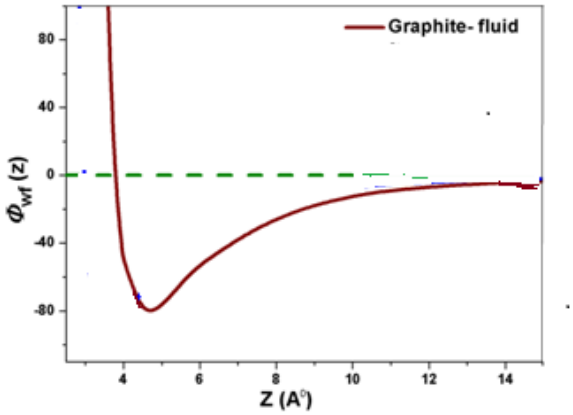

Fig.2 Wall-fluid interaction of 9-3 Steele potential

3.2 Simulation detail

In this work, molecular simulation is performed using grand-canonical transition-matrix Monte Carlo (GCMC) technique [16,17]. In this approach, Monte Carlo simulations are conducted in standard grand-canonical ensemble, where the simulation volume (V),chemical potential (μ), and simulation temperature (T) are held constant and the particle number (N) or particle density (ρ) and energy (U) changes. The maximum number of particles considered for bulk methane simulation is around 400, except near the critical point where maximum particle numbers are around 800 to minimize any error because of larger fluctuations near the critical point. On the other hand, the maximum number of particles for confined methane is varied from 300 to 1200, depending upon the nanopore width (H). During a simulation, attempted transitions between states of different densities are monitored[18,19.] At regular intervals during a simulation, this

information is used to obtain an estimate of the density probability distribution, which is subsequently used to bias the sampling to low probability densities. Over time, all densities of interest are sampled adequately. The result is an efficient self-adaptive method for determining the density probability distribution over a specified range of densities (typically a range that corresponds to the densities of two potentially coexisting phases). Once a probability distribution has been collected at a given value of the chemical potential (μ_0), histogram reweighting technique[20] is used to shift the probability distribution to other values of the chemical potential using the following relationship:

$$ln\pi(N,\mu) = ln\pi(N,\mu_0) + \beta(\mu - \mu_0)N \tag{23}$$

To determine the coexistence chemical potential, we apply the above relationship to estimate the chemical potential that produces a coexistence probability distribution as shown in figure3. Saturated density of vapour phase is related to the first moment of the vapor peak and saturated density of liquid phase is related to the first moment of the liquid peak of the coexistence probability distribution, $\Pi_c(N)$.

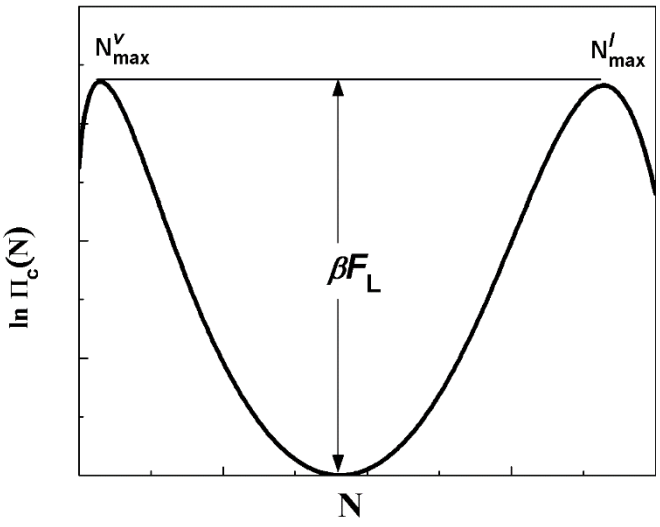

Fig.3 Coexistence probability distribution

To calculate the saturation pressure, we use the following expression:

$$\beta PV = \ln\left[\frac{\sum \pi_c(N)}{\pi_c(0)}\right] - \ln(2) \tag{24}$$

In this work we have estimated the vapor-liquid critical properties by fitting the coexistence densities to the law of the rectilinear diameter[21] and the simplified form of scaling law of the density[22]

$$\rho_l - \rho_v = B(1 - \frac{T}{T_c})^{\beta} \quad (25)$$

$$\frac{\rho_l + \rho_v}{2} = \rho_c + A(1 - \frac{T}{T_c}) \quad (26)$$

where ρ_l, ρ_v, ρ_c, T_c, and β are the liquid-phase density, vapor-phase density, critical density, critical temperature, and critical exponent, respectively. Here, *A* and *B* are fitting parameters.

3.2 Estimation of compressibility factor of saturated liquid and saturated vapor of bulk and confined methane

After knowing the saturated liquid and saturated vapor densities of methane at coexistence from simulation and the critical properties estimates of the methane, the compressibility factor of saturated liquid, saturated vapor of methane is estimated using following expression

$$Z_f = \frac{Pv_l}{RT} = \frac{P}{\rho_l RT} \quad (27)$$

$$Z_g = \frac{Pv_g}{RT} = \frac{P}{\rho_g RT} \quad (28)$$

where *P* is saturated pressure, *T* is saturated temperature, ρ_l and ρ_g are saturated liquid and vapor densities and *R* is universal gas constant.

Critical compressibility factor, Z_c is estimated as

$$Z_c = \frac{P_c v_c}{RT_c} = \frac{p_c}{\rho_c RT_c} \quad (29)$$

where, P_c, ρ_c and T_c are critical pressure, critical density and critical temperature respectively.

CHAPTER-4

Results and Discussion

4.1 Estimation of compressibility factor of bulk methane

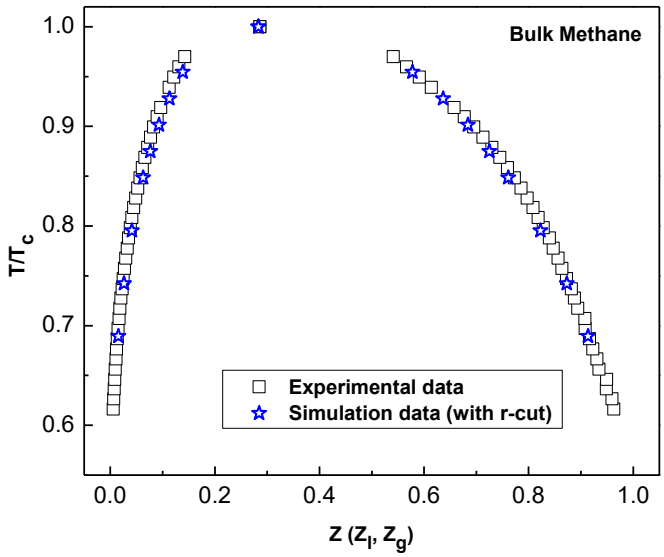

Fig.4 Reduced temperature vs. compressibility factor of saturated liquid and saturated vapor of bulk methane

In this figure we compare experimental data of compressibility factor of saturated liquid and vapor with the corresponding simulation data. It is evident from the figure that experimental and simulation value are in good agreement. The experimental critical compressibility factor (Z_c = 0.288) is in good agreement with the data obtained using molecular simulation. The Z_c value obtained with the simulation is 0.283. This also indicate that the model used for alkane to study the compressibility factor of saturated liquid and vapor is reasonably correct.

4.2 Compressibility factor of methane confined in 40 Å pore width

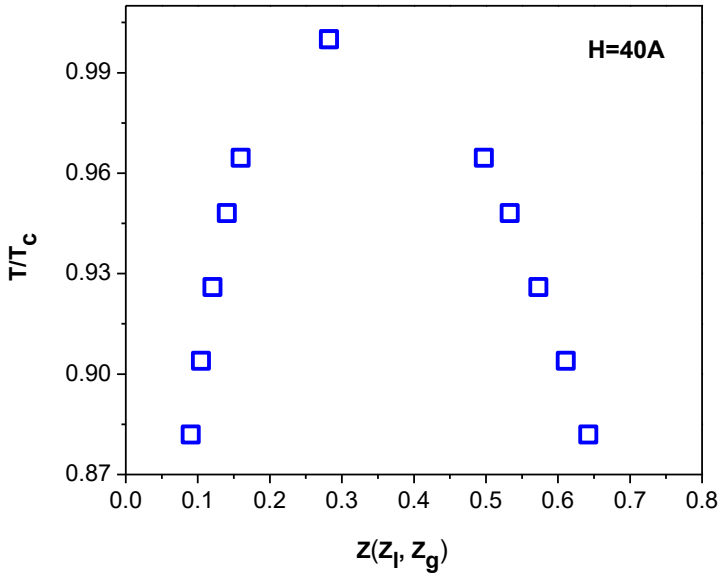

Fig. 5 Reduced temperature vs. compressibility factor of saturated liquid and saturated vapor of methane in 40 Å pore width

Fig.5 shows compressibility factor of saturated liquid (Z_l) and saturated vapor (Z_g) at various reduced temperatures. In this case pore width is 40 Å and the reduced temperature is varied from 0.88 to 0.96.The Z_g decreases with increases in temperature. However the corresponding Z_l of saturated liquid increases with increase in temperature. Moreover the change in Z_l with change in temperature is comparatively smaller with change in Z_g The critical compressibility factor is estimated using critical point data (T_c, ρ_c, P_c) obtained from the simulation. The critical compressibility factor of methane confined in graphite slit pore of 40 Å pore width is 0.282.

4.3 Compressibility factor of confined methane in 30 Å pore width

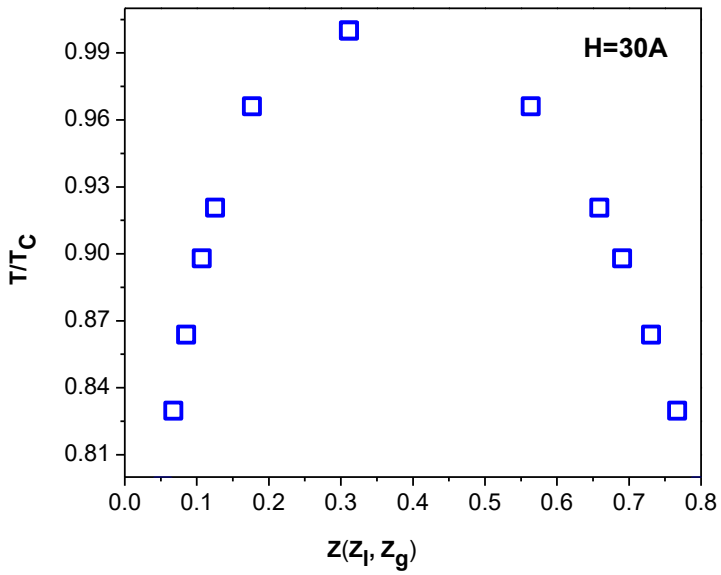

Fig. 6 Reduced temperature vs. compressibility factor of saturated liquid and saturated vapor of methane in 30 Å pore width

Fig.6 shows compressibility factor of saturated liquid (Z_l) and saturated vapor (Z_g) at various reduced temperatures. In this case pore width is 30A and the reduced temperature is varied from 0.79 to 0.96.The Z_g decreases with increases in temperature. However, the corresponding Z_l of saturated liquid increases with increase in temperature. The critical compressibility factor is estimated using critical point data (T_c, ρ_c, P_c) obtained from the simulation data. The critical compressibility factor of methane confined in graphite slit pore of 30 Å pore width is estimated 0.311.

4.4 Compressibility factor of confined methane in 25 Å pore width

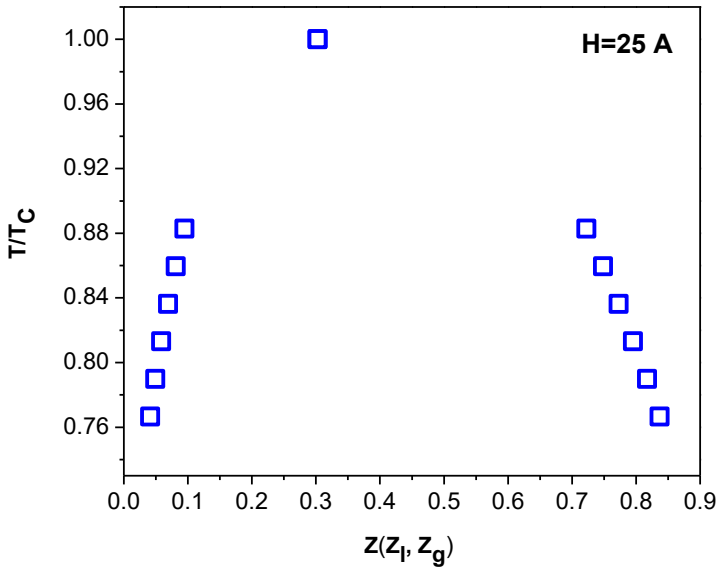

Fig.7 Reduced Temperature vs compressibility factor of saturated liquid and saturated vapor of methane 25 Å pore width

Fig.7 shows compressibility factor of saturated liquid (Z_l) and saturated vapor (Z_g) at various reduced temperatures. In this case pore width is 25 Å and the reduced temperature is varied from 0.76 to 0.88.The Z_g decreases with increases in temperature. However the corresponding Z_l of saturated liquid increases with increase in temperature. Moreover the change in Z_l with change in temperature is comparatively smaller with change in Z_g. The critical compressibility factor is estimated using critical point data (T_c, ρ_c, P_c) obtained from the simulation. The critical compressibility factor of methane confined in graphite slit pore of 25 Å pore width is 0.302.

4.5 Compressibility factor of methane confined in 20 Å pore width

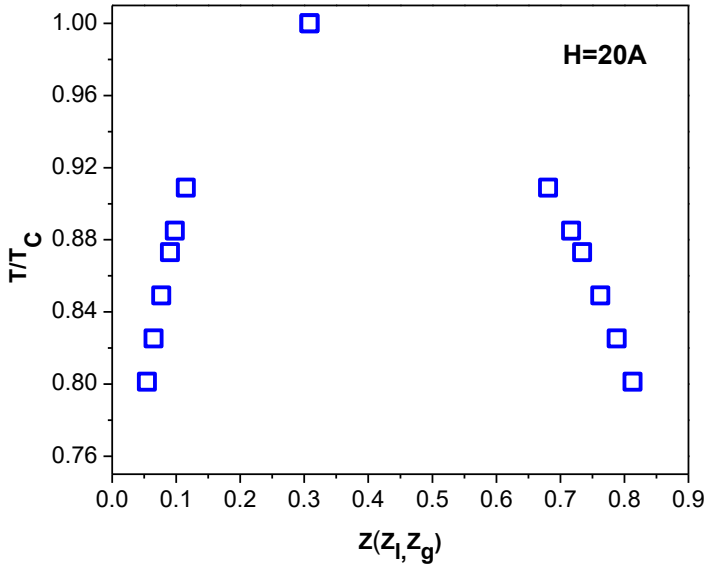

Fig. 8 Reduced Temperature vs compressibility factor of saturated liquid and saturated vapor of methane in 20 Å pore width

Fig.8 shows compressibility factor of saturated liquid (Z_l) and saturated vapor (Z_g) at various reduced temperatures. In this case pore width is 20 Å and the reduced temperature is varied from 0.80 to 0.90. The Z_g decreases with increases in temperature. However, the corresponding Z_l of saturated liquid increases with increase in temperature. Moreover the change in Z_l with change in temperature is comparatively smaller with change in Z_g. The critical compressibility factor is estimated using critical point data (T_c, ρ_c, P_c) obtained from the simulation. The critical compressibility factor of methane confined in graphite slit pore of 20 Å pore width is 0.308.

4.6 Compressibility factor of methane confined in 15 Å pore width

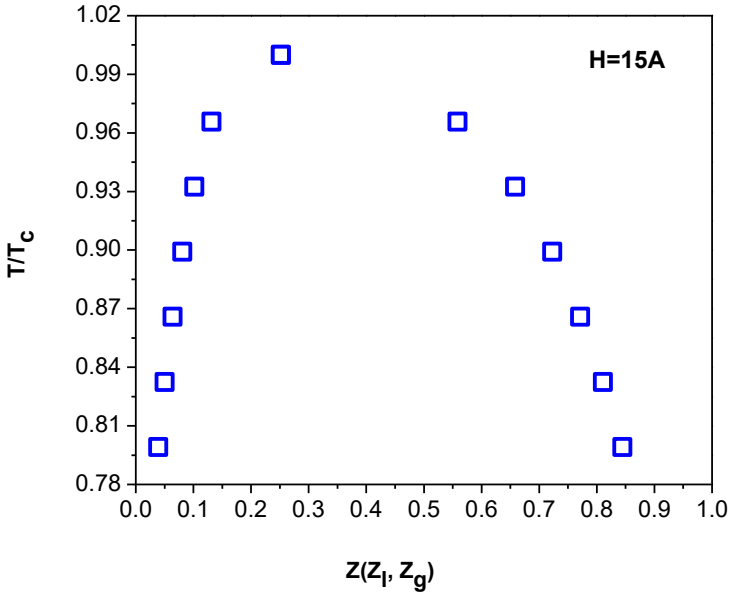

Fig. 9 Reduced Temperature vs compressibility factor of saturated liquid and saturated vapor in 15 Å pore width

Fig.9 shows compressibility factor of saturated liquid (Z_l) and saturated vapor (Z_g) at various reduced temperatures. In this case pore width is 15 Å and the reduced temperature is varied from 0.79 to 0.96. The Z_g decreases with increases in temperature. However the corresponding Z_l of saturated liquid increases with increase in temperature. Moreover the change in Z_l with change in temperature is comparatively smaller with change in Z_g. The critical compressibility factor is estimated using critical point data (T_c, ρ_c, P_c) obtained from the simulation. The critical compressibility factor of methane confined in graphite slit pore of 15 Å pore width is 0.252.

4.7 Compressibility factor of methane confined in 10 Å pore width

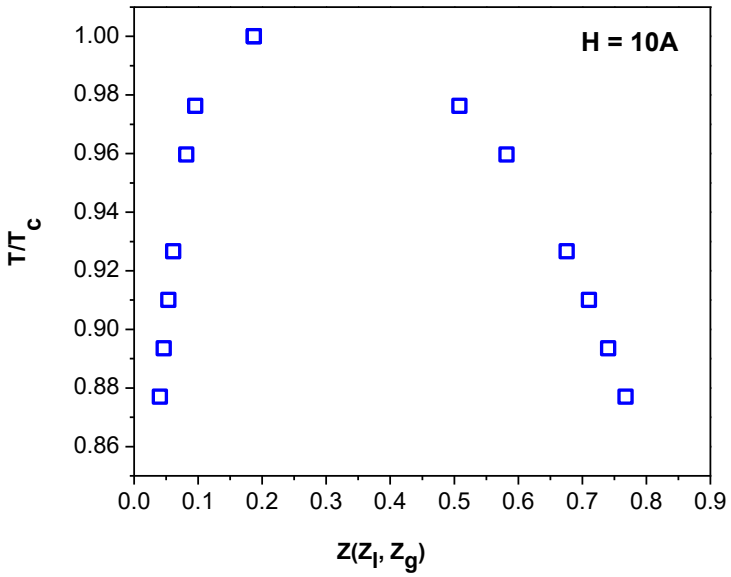

Fig. 10 Reduced Temperature vs compressibility factor of saturated liquid and saturated vapor in 10 Å pore width

Fig.10 shows compressibility factor of saturated liquid (Z_l) and saturated vapor (Z_g) at various reduced temperatures. In this case pore width is 10 Å and the reduced temperature is varied from 0.87 to 0.97. The Z_g decreases with increases in temperature. However the corresponding Z_l of saturated liquid increases with increase in temperature. Moreover the change in Z_l with change in temperature is comparatively smaller with change in Z_g. The critical compressibility factor is estimated using critical point data (T_c, ρ_c, P_c) obtained from the simulation. The critical compressibility factor of methane confined in graphite slit pore of 10 Å pore width is 0.186.

4.8 Compressibility factor of methane confined in 9 Å pore width

.

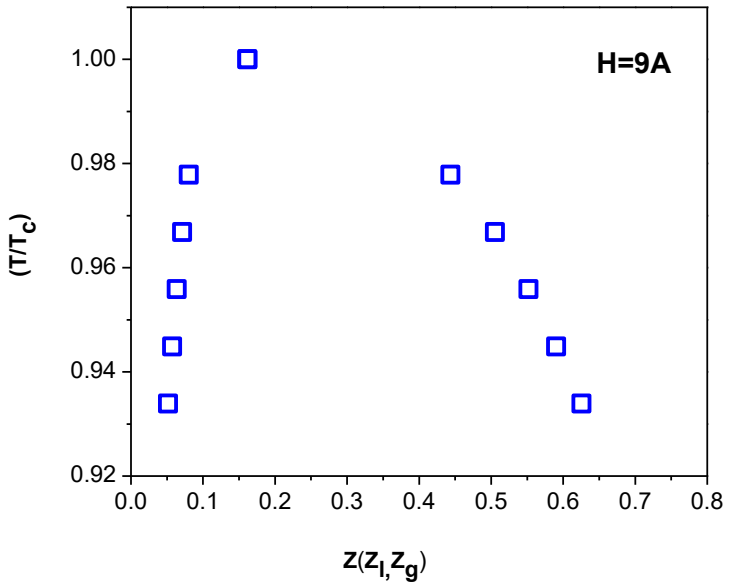

Fig. 11 Reduced Temperature vs compressibility factor of saturated liquid and saturated vapor of methane in H=9 Å

Fig.11 shows compressibility factor of saturated liquid (Z_l) and saturated vapor (Z_g) at various reduced temperatures. In this case pore width is 9 Å and the reduced temperature is varied from 0.93 to 0.97. The Z_g decreases with increases in temperature. However the corresponding Z_l of saturated liquid increases with increase in temperature. Moreover the change in Z_l with change in temperature is comparatively smaller with change in Z_g. The critical compressibility factor is estimated using critical point data (T_c, ρ_c, P_c) obtained from the simulation. The critical compressibility factor of methane confined in graphite slit pore of 9 Å pore width is 0.161.

4.9 Compressibility factor of methane confined in 8 Å pore width

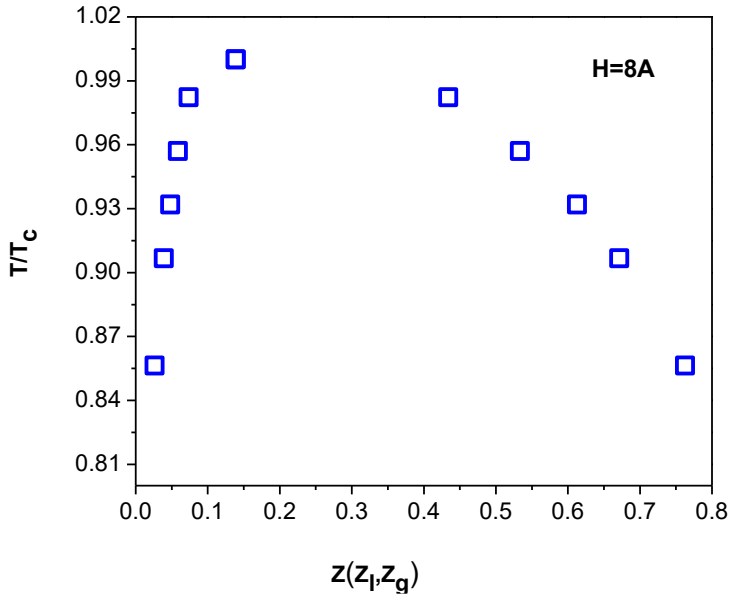

Fig.12 Reduced Temperature vs compressibility factor of saturated liquid and saturated vapor of methane in H=8 Å

Fig.12 shows compressibility factor of saturated liquid (Z_l) and saturated vapor (Z_g) at various reduced temperatures. In this case pore width is 8 Å and the reduced temperature is varied from 0.85 to 0.98. The Z_g decreases with increases in temperature. However the corresponding Z_l of saturated liquid increases with increase in temperature. Moreover the change in Z_l with change in temperature is comparatively smaller with change in Z_g .The critical compressibility factor is estimated using critical point data (T_c, ρ_c, P_c) obtained from the simulation. The critical compressibility factor of methane confined in graphite slit pore of 8 Å pore width is 0.138

4.10 Compressibility factor of methane confined in 6 Å pore width

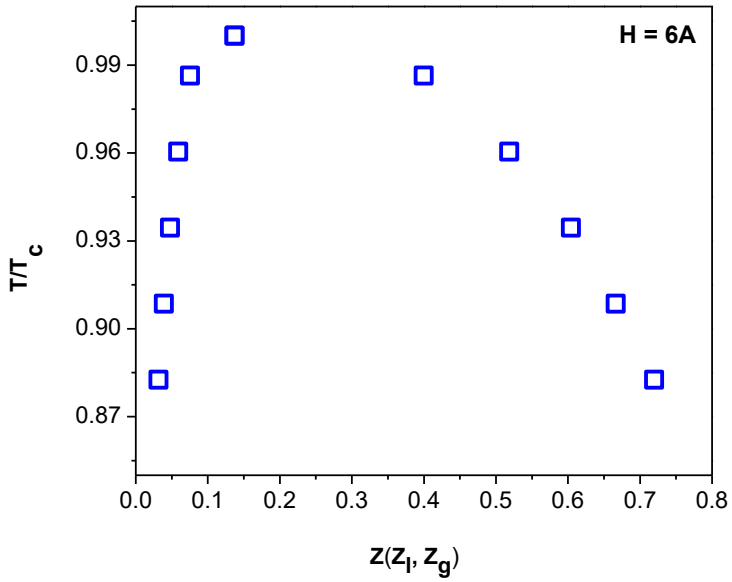

Fig. 13 Reduced Temperature vs compressibility factor of saturated liquid and saturated vapor of methane in H=6 Å

Fig.13 shows compressibility factor of saturated liquid (Z_l) and saturated vapor (Z_g) at various reduced temperatures. In this case pore width is 6Å and the reduced temperature is varied from 0.88 to 0.98. The Z_g decreases with increases in temperature. However the corresponding Z_l of saturated liquid increases with increase in temperature. Moreover the change in Z_l with change in temperature is comparatively smaller with change in Z_g. The critical compressibility factor is estimated using critical point data (T_c, ρ_c, P_c) obtained from the simulation. The critical compressibility factor of methane confined in graphite slit pore of 6 Å pore width is 0.137

4.11 Compressibility factor of methane confined in 5.7 Å pore width

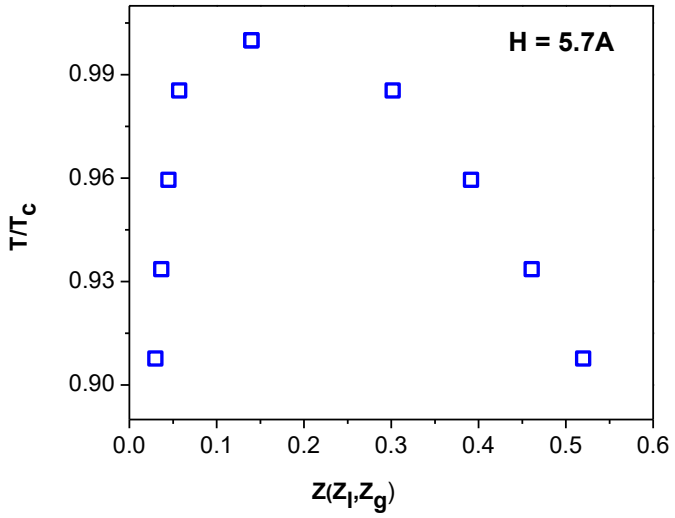

Fig. 14 Reduced Temperature vs compressibility factor of saturated liquid and saturated vapor of methane in H = 5.7 Å

Fig.14 shows compressibility factor of saturated liquid (Z_l) and saturated vapor (Z_g) at various reduced temperatures. In this case pore width is 5.7 Å and the reduced temperature is varied from 0.90 to 0.98. The Z_g decreases with increases in temperature. However the corresponding Z_l of saturated liquid increases with increase in temperature. Moreover the change in Z_l with change in temperature is comparatively smaller with change in Z_g. The critical compressibility factor is estimated using critical point data (T_c, ρ_c, P_c) obtained from the simulation. The critical compressibility factor of methane confined in graphite slit pore of 5.7 Å pore width is 0.140

4.12 Compressibility factor of methane confined in 5.4 Å pore width

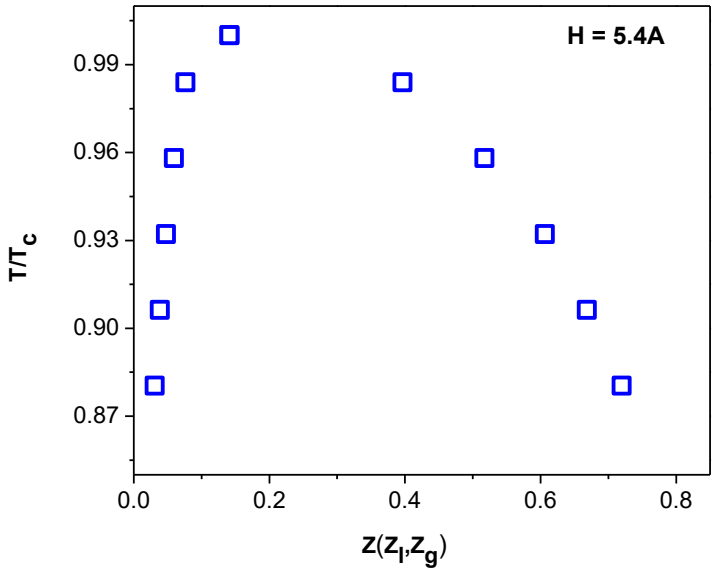

Fig.15 Reduced Temperature vs compressibility factor of saturated liquid and saturated vapor of methane in H=5.4 Å

Fig.15 shows compressibility factor of saturated liquid (Z_l) and saturated vapor (Z_g) at various reduced temperatures. In this case pore width is 5.4 Å and the reduced temperature is varied from 0.88 to 0.98. The Z_g decreases with increases in temperature. However the corresponding Z_l of saturated liquid increases with increase in temperature. Moreover the change in Z_l with change in temperature is comparatively smaller with change in Z_g. The critical compressibility factor is estimated using critical point data (T_c, ρ_c, P_c) obtained from the simulation. The critical compressibility factor of methane confined in graphite slit pore of 5.4 Å pore width is 0.141

4.13 Variation of critical compressibility factor with pore width

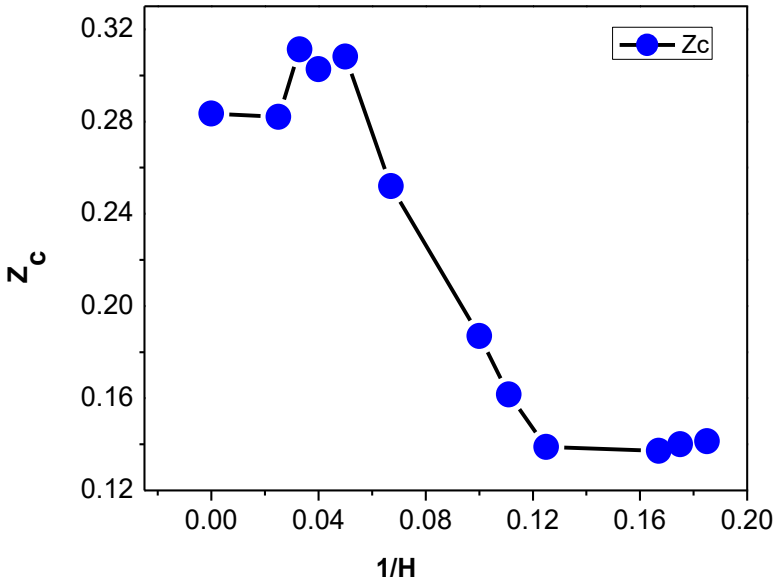

Fig.16 Variation of critical compressibility factor (Z_c) with pore width

This figure shows critical compressibility factor (Z_c) at various pore width (H). Z_c of bulk methane, which correspond to 1/H = 0, is also included for the comparison. The critical compressibility factor of 40 Å is approximately same as the critical compressibility factor of bulk methane. There is a small (10.7%) increase in critical compressibility factor when pore width changes from 40 Å to 30 Å. Moreover, from 30 Å to 20 Å pore width insignificant change in critical compressibility factor is observed. The critical compressibility factor for 20 Å to 8 Å pore width is monotonically decreasing. Further, when pore width changing from 8 Å to 5.4 Å, the critical compressibility factor remains unaltered which indicates quasi-2D behaviour of the confined fluid.

CHAPTER-5

Conclusions

We investigated in this work, the compressibility factor of saturated liquid (Z_l) and vapor (Z_g) and critical compressibility factor (Z_c) of bulk and confined methane. Firstly we compare the experimental data of compressibility factors of saturated liquid and vapor of methane with the corresponding simulation data of current work. The experimental compressibility factor of saturated liquid and vapor and critical compressibility factor of methane are in good agreement with the data obtained using molecular simulation. Further, we have estimated the compressibility factor of saturated liquid and saturated vapor of confined methane at various reduced temperatures in a given pore width. Estimated compressibility factor of saturated liquid increases with increase in temperature and the compressibility factor of saturated vapor decreases with increases in temperature for all studied pore widths, H = 40 Å, 30 Å, 25 Å, 20 Å, 15 Å, 10 Å, 9 Å, 8 Å, 6 Å, 5.7 Å and 5.4 Å. With increase in reduced temperature (T/T_c), change in compressibility factor of saturated liquid is comparatively less than the change in compressibility factor of saturated vapour. Critical compressibility factor is also estimated for all studied pore width using critical point data obtained from the simulation. Variation of Critical Compressibility factor with pore width shows that for bulk methane (i.e., with infinitely large pore width) and with methane in 40 Å pore width remains approximately same. However, from 30 Å to 8 Å pore width the critical compressibility factor is monotonically decreasing and from 8 Å to 5.4 Å it remains almost constant indicating quasi-2D behaviour of confined methane.

CHAPTER-6

REFRENCES

1. Rao, Y. V. C. *Chemical Engineering Thermodynamics*. Universities Press, **1997.**
2. Gelb, L. D., Gubbins, K. E., Radhakrishnan, R., &Sliwinska-Bartkowiak, M., Phase separation in confined systems. *Reports on Progress in Physics*, **1999**, *62*, 1573.
3. Cummings, P. T., Docherty, H., Iacovella, C. R., & Singh, J. K., Phase transitions in nanoconfined fluids. The evidence from simulation and theory. *AIChE journal*, **2010**, *56*, 842-848.
4. Jonsson, U., &Bhushan, B., Measurement of rheological properties of ultrathin lubricant films at very high shear rates and near-ambient pressure. *Journal of applied physics*, **1995**, *78*, 3107-3114.
5. Merlet, C., Rotenberg, B., Madden, P. A., Taberna, P. L., Simon, P., Gogotsi, Y., &Salanne, M., On the molecular origin of supercapacitance in nanoporous carbon electrodes. *Nature materials*, **2012**, *11*, 306-310.
6. Rosenhek-Goldian, I., Kampf, N., Yeredor, A., & Klein, J., On the question of whether lubricants fluidize in stick–slip friction. *Proceedings of the National Academy of Sciences*, **2015**, *112*, 7117-7122.
7. Radhakrishnan, R., Gubbins, K. E., &Sliwinska-Bartkowiak, M., Effect of the fluid-wall interaction on freezing of confined fluids: Toward the development of a global phase diagram. *The Journal of Chemical Physics*,**2000**, *112*, 11048-11057.
8. Largo, J., & Solana, J. R., First-order perturbative contribution to the compressibility factor of square-well fluids from Monte Carlo and integral equation theory. *The Journal of Physical Chemistry B*, **2004**, *108*, 10062-10070.
9. Tang, Y., & Lu, B. C. Y.,An analytical analysis of the square-well fluid behaviors." *The Journal of chemical physics*. **1994**, *100*, 6665-6671.
10. Best, R. B., Zhu, X., Shim, J., Lopes, P. E., Mittal, J., Feig, M., &MacKerell Jr, A. D., Optimization of the additive CHARMM all-atom protein force field targeting improved

sampling of the backbone ϕ, ψ and side-chain χ1 and χ2 dihedral angles. *Journal of chemical theory and computation*, **2012**, *8*, 3257-3273.

11. Apfelbaum, E. M., Vorob'ev, V. S., & Martynov, G. A., Triangle of Liquid− Gas States. *The Journal of Physical Chemistry B*, **2006** , *110*, 8474-8480.
12. Ryckaert, J-P., and André Bellemans., Molecular dynamics of liquid n-butane near its boiling point. *Chemical Physics Letters* **1975**, 30,123-125.
13. Errington, J. R., &Panagiotopoulos, A. Z., A new intermolecular potential model for the n-alkane homologous series.*The Journal of Physical Chemistry B*, **1999**,*103*, 6314-6322.
14. Steele, W. A., The physical interaction of gases with crystalline solids: I. Gas-solid energies and properties of isolated adsorbed atoms. *Surface Science*, **1973**, *36*, 317-352.
15. Porcheron, F., Rousseau, B., Fuchs, A. H., & Schoen, M., Monte Carlo simulations of nanoconfined n-decane films. *Physical Chemistry Chemical Physics*, **1999**, *1*, 4083-4090.
16. Errington, J.R., Evaluating surface tension using grand-canonical transition-matrix Monte Carlo simulation and finite-size scaling. *Physical Review E*, **2003**,*67*, 012102-1,012102-4
17. Errington, J. R., Direct calculation of liquid–vapor phase equilibria from transition matrix Monte Carlo simulation. *The Journal of chemical physics*, **2003**,*118*, 9915-9925.
18. Fitzgerald, M., Picard, R. R., & Silver, R. N., Canonical transition probabilities for adaptive Metropolis simulation. *EPL (Europhysics Letters)*, **1999**, *46*, 282.
19. Fitzgerald, M., Picard, R. R., & Silver, R. N., Monte Carlo transition dynamics and variance reduction. *Journal of Statistical Physics*, **2000**, *98*, 321-345.
20. Ferrenberg, A. M., &Swendsen, R. H., New Monte Carlo technique for studying phase transitions. *Physical review letters*, **1988**, *61*, 2635-.2638
21. Rowlinson, J. S., & Swinton, F., *Liquids and liquid mixtures: Butterworths monographs in chemistry*. Butterworth-Heinemann, **2013**.
22. Rowlinson, J. S., &Widom, B., Molecular Theory of Capillarity (Clarendon, Oxford), **1982.**

M.Sc.Dissertation

ORIGINALITY REPORT

16%	6%	13%	%
SIMILARITY INDEX	INTERNET SOURCES	PUBLICATIONS	STUDENT PAPERS

PRIMARY SOURCES

1	F. Feyzi. "IMPROVING CUBIC EQUATIONS OF STATE FOR HEAVY RESERVOIR FLUIDS AND CRITICAL REGION", Chemical Engineering Communications, 1998 Publication	7%
2	spectrum.library.concordia.ca Internet Source	2%
3	www.cheric.org Internet Source	2%
4	www.coursehero.com Internet Source	2%
5	Ezat Keshavarzi, Mohammad Kamalvand. "Energy Effects on the Structure and Thermodynamic Properties of Nanoconfined Fluids (A Density Functional Theory Study)", The Journal of Physical Chemistry B, 2009 Publication	1%
6	Vinš, Václav, Barbora Planková, Jan Hrubý, and David Celný. "Density gradient theory combined with the PC-SAFT equation of state	<1%

used for modeling the surface tension of associating systems", EPJ Web of Conferences, 2014.
Publication

7	Xiuqin Dong, Xiaoxiao Guan, Yuan Jiang, Jing Ma, Minhua Zhang. "Extension of the TraPPE-UA force field to the simulation of vapor–liquid phase equilibria of vinyl acetate system", Journal of Molecular Liquids, 2015 Publication	<1%
8	S.N. Biswas, C.A.Ten Seldam. "Determination of the coexistence curve of sulfur hexafluoride from isochoric intercepts", Fluid Phase Equilibria, 1989 Publication	<1%
9	Jongcheon Lee, Hwayong Kim. "An equation of state for hydrogen fluoride", Fluid Phase Equilibria, 2001 Publication	<1%
10	Satoru Kato. "Prediction of Henry's constants for alkane/alkane binaries above solute critical", AIChE Journal, 2005 Publication	<1%
11	esperia.iesl.forth.gr Internet Source	<1%